Redox Biology 28 (2020) 101333

Contents lists available at ScienceDirect

Redox Biology

journal homepage: www.elsevier.com/locate/redox

Research Paper

The nitroxide 4-methoxy-tempo inhibits the pathogenesis of dextran sodium sulfate-stimulated experimental colitis

Belal Chami[a,1], Patrick T. San Gabriel[a], Stephen Kum-Jew[a], XiaoSuo Wang[a], Nina Dickerhof[b], Joanne M. Dennis[a], Paul K. Witting[a,*]

[a] Discipline of Pathology, Charles Perkins Centre, Faculty of Medicine and Health, The University of Sydney, NSW, 2006, Australia
[b] Centre for Free Radical Research, Department of Pathology and Biomedical Science, University of Otago Christchurch, Christchurch, New Zealand

ARTICLE INFO

Keywords:
Inflammatory bowel disease
MALDI-Mass imaging
Multiplex fluorescent imaging
Acute experimental colitis

ABSTRACT

Inflammatory bowel disease (IBD) is a chronic condition characterised by leukocyte recruitment to the gut mucosa. Leukocyte myeloperoxidase (MPO) produces the two-electron oxidant hypochlorous acid (HOCl), damaging tissue and playing a role in cellular recruitment, thereby exacerbating gut injury. We tested whether the MPO-inhibitor, 4-Methoxy-TEMPO (MetT), ameliorates experimental IBD. Colitis was induced in C57BL/6 mice by 3% w/v dextran-sodium-sulfate (DSS) in drinking water *ad libitum* over 9-days with MetT (15 mg/kg; via *i. p.* injection) or vehicle control (10% v/v DMSO + 90% v/v phosphate buffered saline) administered twice daily during DSS challenge. MetT attenuated body-weight loss (50%, $p < 0.05$, n = 6), improved clinical score (53%, $p < 0.05$, n = 6) and inhibited serum lipid peroxidation. Histopathological damage decreased markedly in MetT-treated mice, as judged by maintenance of crypt integrity, goblet cell density and decreased cellular infiltrate. Colonic $Ly6C^+$, MPO-labelled cells and 3-chlorotyrosine (3-Cl-Tyr) decreased in MetT-treated mice, although biomarkers for nitrosative stress (3-nitro-tyrosine-tyrosine; 3-NO_2-Tyr) and low-molecular weight thiol damage (assessed as glutathione sulfonamide; GSA) were unchanged. Interestingly, MetT did not significantly impact colonic IL-10 and IL-6 levels, suggesting a non-immunomodulatory pathway. Overall, MetT ameliorated the severity of experimental IBD, likely via a mechanism involving the modulation of MPO-mediated damage.

1. Introduction

Inflammatory Bowel Disease (IBD) is characterised by relapsing and remitting inflammation in the gastrointestinal tract. The three IBD subtypes; Crohn's disease (CD), ulcerative (UC) and indeterminate colitis are characterised by focal and chronic inflammation that yields irreversible structural and functional changes to the bowel. The precise cause of IBD is unknown and likely multifactorial, however, it is accepted that a dysregulated immune response is causally linked to disease progression [62]. Risk factors contributing to IBD pathogenesis include: family history, ethnicity and environmental factors such as use of non-steroidal anti-inflammatory drugs (NSAIDs), infective proctocolitis and smoking [21].

Symptoms of IBD are notoriously debilitating and include chronic diarrhoea, weight loss, malaise, fever and abdominal pain. Nutritional deficiencies and anaemia are common and extra-intestinal manifestations include retarded growth, musculoskeletal pain, arthritis, liver disease, urologic complications and inflammatory and necrotising skin conditions [39,60]. Up to 90% of CD [29] and 35% of UC patients [11] require surgical intervention [32]. Recurrent IBD significantly affects productivity and morbidity; IBD continues to represent a serious chronic disease burden in health systems worldwide [59,64].

A striking histological feature associated with inflammation in IBD is neutrophil infiltration [51], particularly during disease relapse. The mechanism whereby pro-inflammatory infiltrates are recruited to the colon is largely unknown, though likely involves induction of cellular chemotactic mediators that signal immune cells within the vasculature. Reactive oxygen species (ROS) produced via tissue damage and/or inflammatory processes (*e.g.*, oxidative burst) are established activators of key pro-inflammatory signalling cascades. Thus, local tissue damage and/or ROS production can drive a cycle of sustained immune cell recruitment and host-tissue injury to promote inflammation and amplify oxidative stress. Accordingly, ROS-induced oxidative damage appears to be involved in several chronic and inflammatory diseases, including in IBD [2].

The haem enzyme myeloperoxidase (MPO) is primarily found in

* Corresponding author.
E-mail address: paul.witting@sydney.edu.au (P.K. Witting).
[1] Current address: Discipline of Oral Pathology, Sydney Dental School, The University of Sydney, NSW, 2006, Australia.

https://doi.org/10.1016/j.redox.2019.101333
Received 17 June 2019; Received in revised form 24 September 2019; Accepted 26 September 2019
Available online 28 September 2019

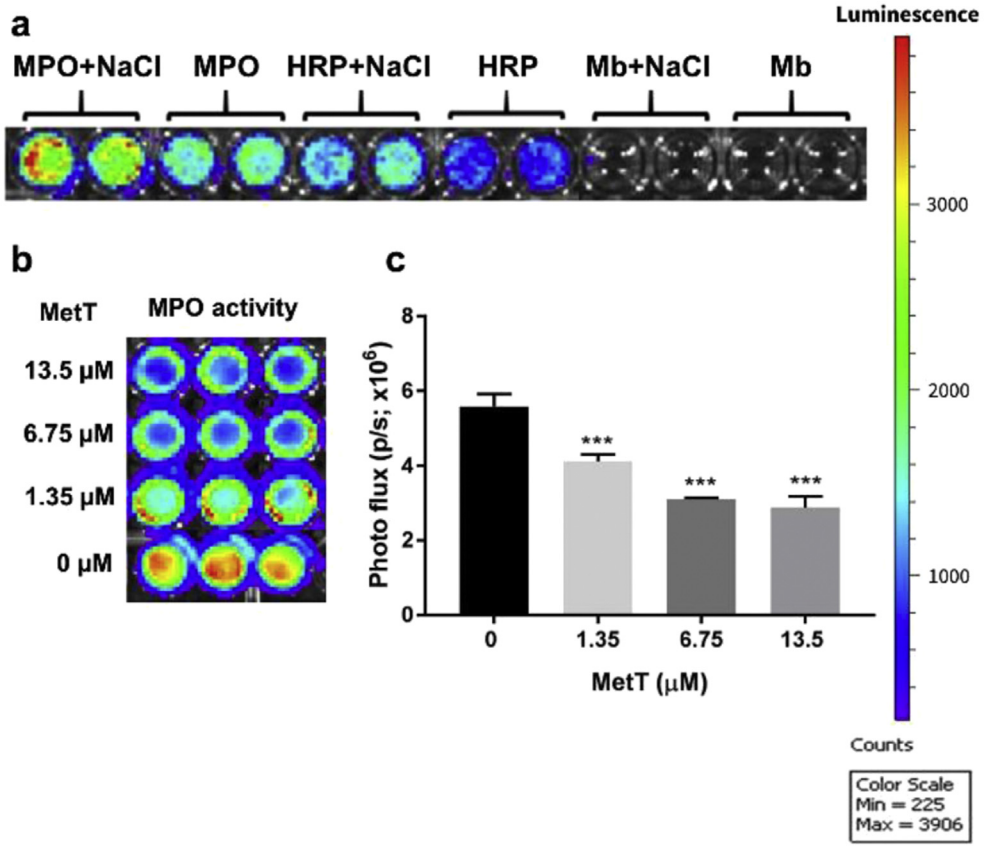

Fig. 1. MetT inhibits MPO/HOCl-mediated oxidation of luminol in an isolated system. Bioluminescence emitted from (a) MPO-, HRP- and Mb-mediated oxidation of luminol in the presence and absence of supplemented NaCl (750 mM). Panel (b) Representative and c) quantitative analysis of MPO activity (with NaCl added) with 1.35 µM, 6.75 µM & 13.5 µM MetT. Vertical scale to the right of images refers to the relative luminescence radiance presented as a heat map. Different to the vehicle; $^{***}p < 0.001$. All data is representative of 3 experimental repeats. Data represents n = 3 for data shown in panel (c).

neutrophil granulocytes (and to a lesser extent in macrophages) and produces hypochlorous acid (HOCl), a powerful two-electron oxidant that damages a range of biological targets [30,47]. Extracellular production of HOCl is implicated in several inflammatory diseases and may promote oxidative damage and inflammation in IBD. Biomarkers for MPO-mediated damage include 3-chlorotyrosine (3-Cl-Tyr) [30] and glutathione sulfonamide [27,28]. Notably, 3-Cl-Tyr levels are markedly elevated in the colon and circulation [37], while faecal MPO correlates with disease severity [51] in patients with IBD. Recently, the pathophysiological role of MPO in IBD has been explored, where MPO-mediated HOCl production was considered to enhance local tissue injury and exacerbate inflammation [15].

Targeting oxidative damage, including that mediated by the MPO/H_2O_2/halide enzyme system, may be an effective strategy to modulate inflammation in IBD. MPO is a professional peroxidase, carrying a ferric haem (MPO-Fe(III)), which in its resting/native state consumes H_2O_2 to transition into compound I. MPO can then oxidise halogens (*i.e.*, the physiologically abundant Cl^- anion), thus returning to its native state, producing HOCl [30]. Cyclic nitroxides are cell-permeable stable free radicals documented widely for their broad antioxidant activity [62]. Nitroxides exhibit superoxide dismutase- and catalase-like activities [20], and compete with H_2O_2 for redox active metals to prevent Fenton-type chemistry [33]. Nitroxides also accept electrons from mitochondrial electron transport-chain proteins, thereby inhibiting pathological ROS accumulation [33]. For example, mitochondrial-targeted nitroxides have been used to inhibit radiation-induced injury to human skin [12]. These beneficial activities are associated with reduced lipid, protein oxidation and DNA damage, and also enhanced bioavailability of nitric oxide (NO) *in vitro*. Further, cyclic nitroxides such as TEMPOL (4-hydroxy-2,2,6,6-tetra-methylpiperidine-1-oxyl), are well tolerated and show low pharmacotoxicity in animal models [3,48] and nitroxide-based formulations are in clinical use for radiation-induced alopecia in humans [16,41].

In addition to their documented ability to scavenge reactive oxidants, cyclic nitroxides are substrates for catalytically active MPO [34,49] and are potent inhibitors of hypohalous oxidant production by the MPO/H_2O_2/halide cycle [48]. Thus, while nitroxides effectively react with MPO compound I to form compound II, they react relatively poorly with compound II allowing accumulation of MPO in this ferryl-Fe form. Unlike MPO compound I, MPO compound II does not oxidise halides [17] thus, hypohalous acid formation is abrogated in the presence of nitroxides. In addition, TEMPOL inhibits MPO-mediated reactive nitrogen species formation via rapid reaction with $^{\bullet}NO_2$, thereby inhibiting MPO-mediated RNase and protein nitration [55].

Cyclic nitroxides also show combined anti-inflammatory and antioxidant activities *in vivo* that are pertinent to prevention of gastrointestinal damage. For example, TEMPOL inhibits indomethacin-induced gastric damage in rats [18] and attenuates all indices of inflammation in a carrageenan-induced inflammation model, including nitration and oxidation of proteins [48]. Further, TEMPOL protects purinergic neuromuscular transmission and improves propulsive motility in animal models of colitis [50]. However, the potential of cyclic nitroxides to modulate inflammation and MPO/HOCl-induced damage associated with IBD has not been specifically studied. Herein, we examined the ability of the cyclic nitroxide derivative, 4-Methoxy-TEMPO (MetT), to ameliorate dextran sodium sulfate (DSS)-induced colitis in mice through inhibition of MPO activity.

2. Results

2.1. MetT attenuates the HOCl-mediated oxidation of luminol ex vivo

Our data indicate that luminol is preferentially oxidised by the two-electron oxidant HOCl which is produced by peroxidases, chiefly, MPO in the presence of H_2O_2 and excess Cl^- ion. Thus, MPO significantly increased the luminol oxidation in the presence of NaCl, emitting

luminescence signal ~3800 radiance compared to a signal ~1400 radiance in the absence of NaCl (Fig. 1a). By contrast, horseradish peroxidase (HRP) registered only a marginally higher luminescence signal ~1200 radiance with added NaCl, compared to ~800 radiance signal obtained in the absence of added salt. HRP is capable of oxidising free Cl^- to give HOCl, albeit with a rate constant for reaction significantly less than MPO [31]. Myoglobin (Mb) is a non-professional peroxidase with poor catalytic efficiency [63], and no reported chlorinating activity. Consistent with this notion, virtually no luminescent signal was detected in mixtures of Mb and luminol with and without added NaCl, suggesting that luminol is oxidised by the chlorinating activity of peroxidases rather than their peroxidase activity *per se*. Furthermore, it is very likely that purified MPO and HRP contains trace levels of Cl^- (from the manufacturing process) which may account for baseline levels of luminol oxidation that increased with added NaCl.

Addition of MetT attenuated luminol oxidation (in the presence of NaCl) (Fig. 1b) consistent with the nitroxide inhibiting MPO enzymic activity. Titrating MetT (final concentrations: 1.35 μM, 6.75 μM and 13.5 μM) ameliorated luminol oxidation by 28%, 45% and 50%, respectively (Fig. 1c) indicating a dose-dependent inhibition of MPO by the added nitroxide. Whether the added 4-MetT directly scavenged HOCl in addition to inhibiting MPO enzymic turnover has not been explored here and remains a possibility. Nevertheless, production of HOCl by MPO is abrogated by the presence of the added nitroxide.

2.2. MetT improves clinical parameters in mice challenged with DSS

To examine whether MetT administration ameliorated experimental colitis, mice were challenged with 3% w/v DSS in drinking water for 9 days. Mice assigned to the MetT (15 mg/kg) or vehicle (dimethyl sulfoxide; control) groups were injected (*i.p.*) twice daily during the course of DSS insult. No change in drinking consumption was noted between any treatment group throughout the study duration (data not shown). Body weight loss is proportional to the colitis severity [14] and was used as a clinical biomarker in this study. No significant body weight loss was noted between groups until day 9 of DSS insult. At this time point, mice challenged with DSS alone showed an average of 14% decrease in body weight relative to control mice receiving normal drinking water (Fig. 2a). Mice co-administered MetT and DSS showed a significant reduction in body weight loss (8%; $p < 0.05$) than mice treated with DSS alone (vehicle control) at the same time point. No differences in body weight were observed in mice provided normal drinking water treated with either vehicle or MetT alone, consistent with the nitroxide being well-tolerated by the mice. Together this data suggests that MetT attenuates the severity of DSS-induced colitis.

Features of murine colitis include reduced mobility, faecal consistency and rectal bleeding. In the absence of DSS, mice in the vehicle-control and MetT groups did not register any measurable clinical scores at day 9 of the study (Fig. 2b). Mice challenged with DSS showed increased clinical scores at day 9 post-challenge ($p < 0.05$). By contrast, mice co-treated with DSS and MetT showed an ameliorated clinical score (~45% decrease; $p < 0.05$) compared to mice treated with DSS alone, indicating that MetT mitigated colitis.

Colon 'crypt dropout' is a pathological feature of colitis and is characterised by a progressive shift in the crypt apex from the basement membrane until crypts eventually drop out of the *lamina propria* [23]. Overall, crypts amounted to ~40% of the total colon area per field of view in mice receiving normal water (irrespective of added vehicle or MetT) (Fig. 2c). Mice treated for 9 days with DSS showed a significant decrease in crypt number (~422) relative to the vehicle-control. However, DSS-challenged mice co-treated with MetT consistently showed significantly higher crypt content compared to the gut samples obtained from vehicle control DSS-treated mice, further suggesting that MetT administration attenuates DSS-mediated colon damage.

Goblet cells are closely associated with crypt structures and are depleted during crypt dropout [23]. Representative staining of mucin, a glycosylated protein produced by goblet cells, showed a marked loss in the colon of DSS-treated mice compared to normal drinking water controls (Fig. 2d). DSS-stimulated decrease in mucin was noticeably inhibited in mice co-administered with MetT. Software-based quantification revealed significantly decreased levels of mucin along the length of the transverse and descending colon in DSS-treated mice, when compared to normal water-treated counterparts (Fig. 2e). Mucin levels decreased ~11-fold in DSS-treated mice. By contrast, mucin staining decreased only ~2-fold in mice co-administered DSS and MetT, indicating that MetT preserved both crypt integrity and colon epithelia during the course of experimental colitis.

2.3. Administered MetT is absorbed systemically and is localised in the colon

Matrix-assisted laser desorption/ionisation mass spectrometry (MALDI-MS) was performed on fresh-frozen colon from DSS and DSS + MetT treated mice. A heat map showed registration of the MetT parent ion (mass ion 186 *m/z* representing positively charged MetT) at the 8% colour threshold in a DSS + MetT mouse colon, while the positive signal was completely absent in mice treated with DSS-alone at the same threshold setting. Heat maps generated from the colon of mice in the DSS + MetT group demonstrates that the drug co-localised to the colonic tissue area as determined by H&E staining on the same tissue section. Collectively, these data indicated that MetT accumulated within the colonic tissue of mice (Fig. 3).

2.4. Histopathological evidence that DSS-induced colitis is attenuated by MetT

Following immunohistochemistry, quantification of cellular infiltrates (total number of nuclei), MPO^+ cells and crypts in the colon was performed using software-based tissue segmentation algorithms to map histological features, as shown in Supplementary Fig. S1. Consistent with DSS-mediating inflammation in the colon [14], the total number of nuclei mapped to the colon increased in DSS-treated mice, when compared to mice treated with normal drinking water (vehicle) or with MetT alone (Fig. 4a & Supplementary Fig. S2). By contrast, nuclei mapping in DSS-treated mice co-supplemented with MetT appeared less dense than vehicle counterparts (Supplementary Fig. S2), suggesting that MetT diminished DSS-induced immune cell chemotaxis.

While both DSS-treated vehicle and MetT mice showed significantly increased levels of total cellular infiltrate compared to control counterparts, MetT administration significantly reduced the extent of DSS-mediated cellular infiltration (Fig. 4a). Overall, immune-positive MPO^+ pixel intensity increased significantly during the course of DSS-induced colitis and were attenuated to near baseline levels with MetT administration (Fig. 4b). The severity of DSS-induced colitis is positively correlated to colonic MPO levels [57]. Similar analyses indicated that crypt integrity negatively correlated with MPO levels ($p = 0.011$, Fig. 4c), indicating that MPO adversely affected crypts and that the maintenance of crypt integrity provided by MetT supplementation is likely mediated through its action on MPO. These data support the idea that MPO inhibition is a critical activity for cyclic nitroxides such as MetT and that this is strongly linked to the amelioration of DSS-induced colitis in mice.

2.5. MetT decreases immune cell infiltration in the colon of mice treated with DSS

To identify the phenotypes of infiltrating cell populations in the inflamed colon, positively labelled $Ly6C^+$ monocytes, $Ly6G^+$ neutrophils, and $F4/80^+$ macrophages (Fig. 5), were quantified in the colon *submucosa* and *lamina propria*. MPO was also co-labelled with monocytes, neutrophils and macrophages to assess the primary source of colonic MPO. Interestingly, monocytes showed the highest level of

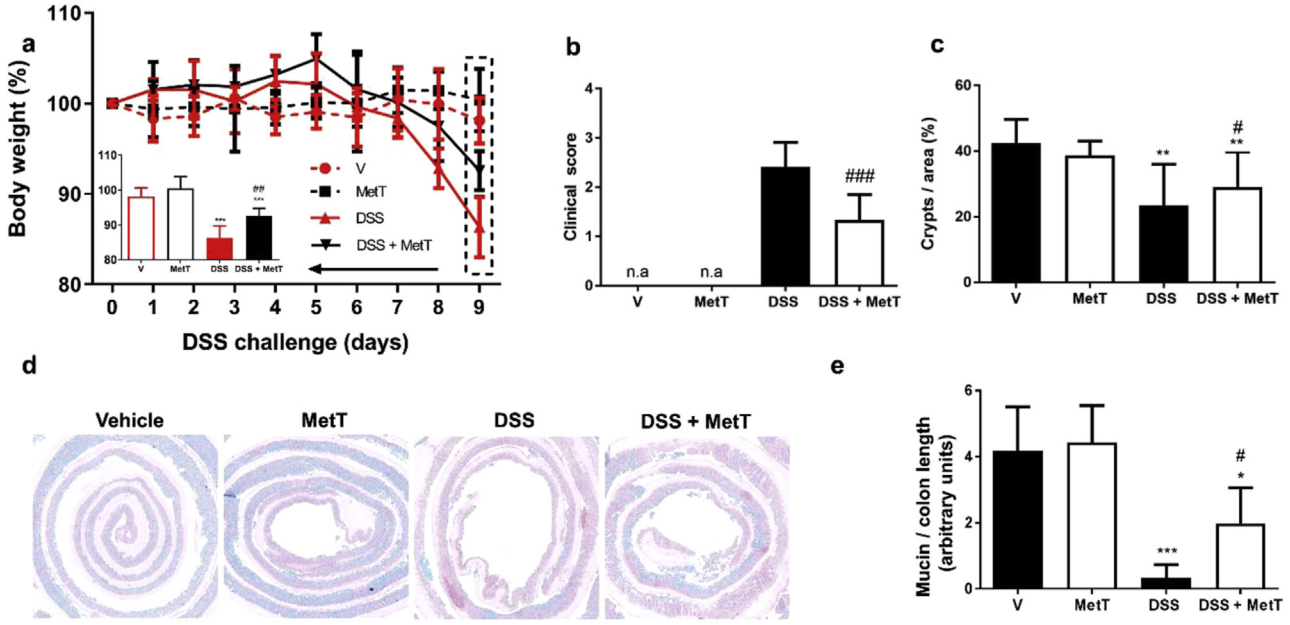

Fig. 2. MetT attenuates body weight loss, and clinical and histopathological parameters in mice challenged with DSS in the drinking water. Mice exposed to normal water or 3% w/v DSS were treated with vehicle or MetT (15 mg/kg), twice daily by *i. p.* injection over 9 days. Panel (a) Percent body weight loss in mice over 9-days DSS insult. Data is expressed as the percentage of the original weight prior to treatment. Panel (b) Enumerated clinical score representing reduced mobility, faecal consistency and rectal bleeding in mice at day 9 of DSS challenge. Panel (c) Pattern-based recognition of intact crypts (InForm V2.1.1), as represented by percent fractional area of the total colonic mucosa area in the same colon section following sacrifice at day 9 of DSS challenge. Crypt drop out was assessed using a histological Alcian blue stain for mucin after 9 days of DSS-insult. Panel (d) Representative Alcian blue and Safranin O staining in control mice and following DSS-induced colitis with and without MetT treatment. Panel (e) Software-based quantification (MetaMorph® V7.8) of the extent of Alcian blue staining included the transverse and descending regions of the colon that was subsequently normalised to the combined length of the aforementioned regions. Slides were imaged with a Zeiss Axio Scan. Z1 slide scanner and pseudo-fields of view were obtained at 1x magnification. Data represents mean ± SD; n = 6 mice per group and corresponding n = 6 data points except for (c), where n > 70 based upon the analysis of each field of view at 20x magnification. Different to vehicle, where $^{*}p < 0.05$, $^{**}p < 0.005$ & $^{***}p < 0.001$. Different to DSS group, where $^{\#}p < 0.05$, $^{\#\#}p < 0.005$ & $^{\#\#\#}p < 0.001$. n. a. = not applicable. (For interpretation of the references to colour in this figure legend, the reader is referred to the Web version of this article.)

MPO co-staining followed by neutrophils, with only a relatively small fraction of F4/80 positive macrophages co-staining for MPO (Fig. 5a–b, e-h & i-j, respectively).

Similar to our previous investigation [14], DSS-induced colitis resulted in significant monocyte and neutrophil recruitment to the inflamed colon tissue, while macrophages showed a trend to increase in the colon, when compared to mice in the absence of DSS (see panels Fig. 5m, n and o, respectively). Co-administration of MetT during DSS-stimulated colitis significantly attenuated the numbers of monocytes recruited to the inflamed colon, however, the level of macrophage and neutrophil recruitment remained unaltered (compare panels Fig. 5m, n and o, respectively).

Macrophages (anti-F4/80 antibody), neutrophils (anti-Ly6G), monocytes (anti-Ly6C), and the haem enzyme MPO (anti-MPO) were labelled simultaneously and each of these cell types were mapped to the tissue by the visualisation of their respective antibody; co-localisation of MPO^{+} staining was consistent with the haem protein being present in all three of these infiltrating cell types (Supplementary Fig. S2). Mapping of these cell types in the colon tissue revealed differential cell densities and local distributions (Supplementary Fig. S2).

Spatial cell phenotyping revealed a differential pattern of macrophage infiltration in the colon of DSS-treated mice. Specifically, macrophage populations (red dots) tended to reside in the *topical lamina propria* region of the colon from DSS-treated mice in the absence of MetT (Supplementary Fig. S2l), whereas macrophage populations were most dense in the *basal lamina propria* and *submucosal* sub-region of the colon in DSS-treated mice that were also co-supplemented with MetT (Supplementary Fig. S2p). While macrophage migration in the colon was demonstrated to be affected by MetT, little difference in overall macrophage density was noted in the colons of DSS-challenged mice in the absence or presence of MetT (Supplementary Fig. S2 panels l and p, respectively). Neutrophil (blue dots) migration appeared to be altered to a similar extent to that for macrophages, *i.e.,* neutrophils showed a stronger tendency toward a *basal lamina propria/submucosal* distribution in colons isolated from DSS-treated mice in the presence of MetT. Overall monocyte (yellow dots) density decreased in colons from DSS-treated mice in the presence of MetT (compare panel Figure 5m and Supplementary Fig. S2p). It is unclear whether MetT influenced immune cell migratory patterns in the inflamed colon directly via attenuating histoarchitectural pathology or indirectly through the inhibition of MPO production of HOCl. Taken together these data suggests that attenuation of immune cell infiltration, in particular monocyte recruitment, in DSS-induced colitis by MetT correlates with reduced MPO and further indicates that MetT exhibits an anti-inflammatory activity that acts in concert with antioxidant activity in this animal model.

2.6. MetT attenuates DSS-induced protein modification

Levels of glutathione sulfonamide (GSA) were determined as a marker of HOCl-mediated glutathione oxidation [27,28]. Overall, GSA levels increased significantly in DSS-challenged mice when compared to their respective normal water-treated counterparts (Fig. 6a). However, co-administration of DSS + MetT had no material affect on GSA levels when compared to DSS alone. By contrast, 3-Cl-Tyr, a specific marker of HOCl-mediated protein oxidation was significantly increased in DSS treated mice (in the absence of the nitroxide), and was abrograted markedly to below baseline levels in DSS + MetT mice, when compared to corresponding controls (Fig. 6b). These data show that nitroxide decreases MPO/HOCl-specific protein damage in the colon but is unable

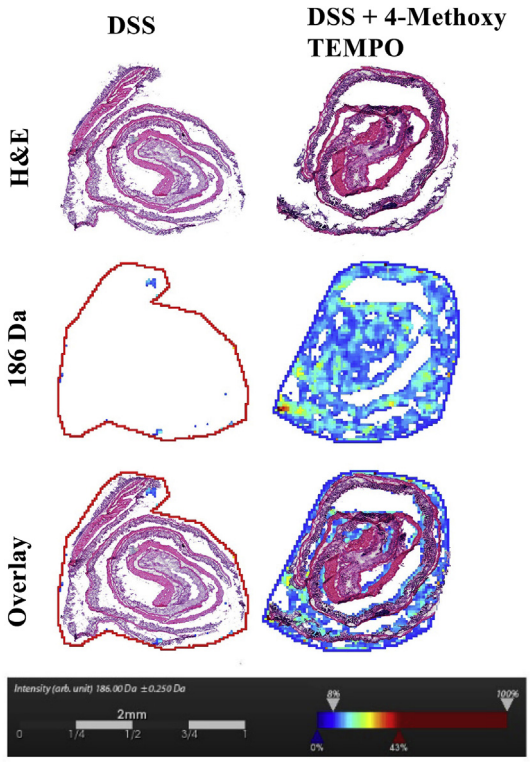

Fig. 3. Matrix-assisted laser desorption/ionisation mass spectrometry (MALDI-MS) detection of MetT in mice colon following 9 days of DSS challenge. Analysis of the ion 186 Da peak, corresponding to the parent ion of MetT (186 Da), was localised in the colon tissue of a mouse receiving both DSS and MetT, while absent in the DSS-alone treated mouse. Colon tissues were subsequently retrieved post-MALDI-MS analysis, stained with H&E and overlayed with the spatial map of the 186 Da MetT parent ion to co-register drug distribution with colon tissue. MALDI-MS was performed with mass range restricted to 100–2000 a.m.u. while under 8% laser power, 1000 Hz and a raster width of 50 μm. Colour scale (bottom) refers to the relative mass intensity for a given mass-charge (m/z = 186 a.m.u.) ratio presented as a heat map. (For interpretation of the references to colour in this figure legend, the reader is referred to the Web version of this article.)

to inhibit oxdiative modification of low-molecular weight thiols.

Circulating lipid hydroperoxide (LOOH) can represent a biomarker of inflammation-induced damage and is increased significantly during DSS-induced colitis [5]. Herein, acute inflammation associated with DSS-induced colitis significantly increased serum levels of LOOH by ~1.5-fold compared to normal drinking water controls. This increase was ameliorated by supplementation with MetT (Fig. 6c). This data suggests that MetT was absorbed systemically and enhanced overall (plasma) antioxidant status in DSS-challenged mice.

Superoxide radical anion (O_2-•) rapidly reacts with NO to yield the potent oxidant peroxynitrite ($ONOO^-$) [9] and subsequently the oxidation product, 3-nitro-tyrosine (3-NO_2-Tyr) [10]. Interestingly, DSS-induced colitis did not increase 3-NO_2-Tyr levels as determined by immunohistochemistry, when compared to control mice receiving normal drinking water (compare panels Fig. 6d and e). However, administration of the MPO inhibitor, MetT, during the course of DSS-induced colitis significantly increased 3-NO_2-Tyr levels to below baseline (Fig. 6e).

2.7. MetT attenuates in vivo HOCl-mediated bioluminescence of oxidation during DSS-induced colitis

Luminol is a substrate for HOCl, producing a bioluminescent signal at 431 nm [13]. Notably, MPO deficiency abolished bioluminescent co-localisation to histological regions of inflammation in an animal model of acute dermatitis, suggesting luminol oxidation was sensitive to MPO-derived oxidants [26]. At day 7, the abdominal bioluminescent signal from mice treated with DSS + MetT was decreased when compared to DSS alone counterparts (p = 0.053; Fig. 7a and b). This suggests MPO/HOCl-mediated luminol oxidation was attenuated by MetT-mediated inhibition of MPO chlorinating activity. Unsurprisingly, vehicle control mice showed very little abdominal bioluminescence, with a total radiance value of ~5, compared to ~ 30 in mice treated with DSS.

Interestingly, mice treated with vehicle (both control and DSS alone groups) emitted bioluminescence at the site of repeated *i. p.* injection, presumably the result of a local inflammatory response surrounding the *i. p.* site (red arrows; Fig. 7a). A bioluminescent signal was largely absent from the repeated *i. p.* site in mice treated with MetT, suggesting that MetT also abrograted subcutaneous MPO activity.

Furthermore, the bioluminescent signal in mice treated with MetT was again diminished compared to mice treated with vehicle (Supplementary Figs. S3a and b) in a recovery model of DSS-induced colitis. In this second model, mice were challenged with 3% w/v DSS for 4 days, then the extent of DSS challenge was markedly decreased and the mice allowed to recover with 0.003% w/v DSS (effectively normal drinking water) for an additional 6 days. The outcome from this second study suggests that MetT administration also enhances recovery from a bout of acute colitis.

2.8. Effects of MetT on the immunological profile following DSS-induced colitis

Cyclic nitroxides have recently been shown to have

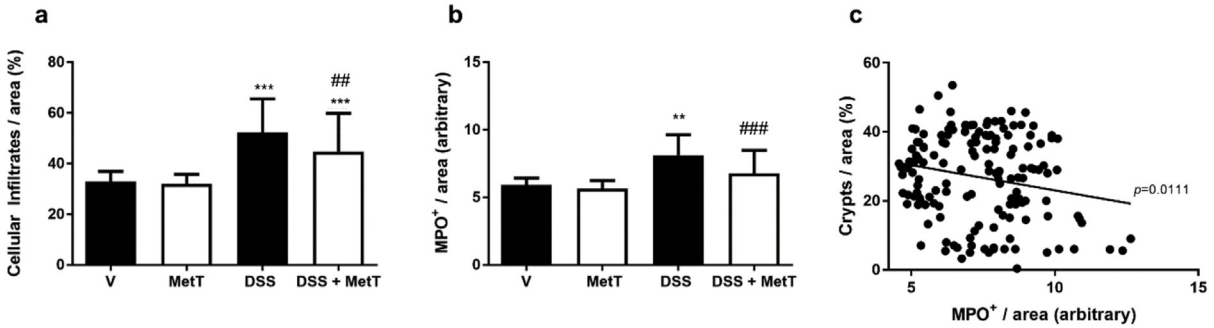

Fig. 4. Software-based analysis of colon histoarchitecture and immunohistochemistry following 9 days of DSS-insult. Panels represent (a) total cellular infiltrates, (b) analysis of MPO levels in the colon as performed in InForm (V2.1.1) and (c) Software-based assessment of crypt integrity correlated to immunohistochemical detection of MPO in the same sectioned tissue. Data represents approximately n = 50–70 fields of view per mouse with data averaged and plotted as mean ± SD; n = 6 mice per group. Intact crypts and cellular infiltrates data are represented as a percentage of total tissue area per field of view in the colon of mice following DSS-challenge. Different to corresponding controls; $^{**}p < 0.01$ and $^{***}p < 0.001$. Different to the DSS group in the absence of MetT; $^{\#\#}p < 0.01$ and $^{\#\#\#}p < 0.001$.

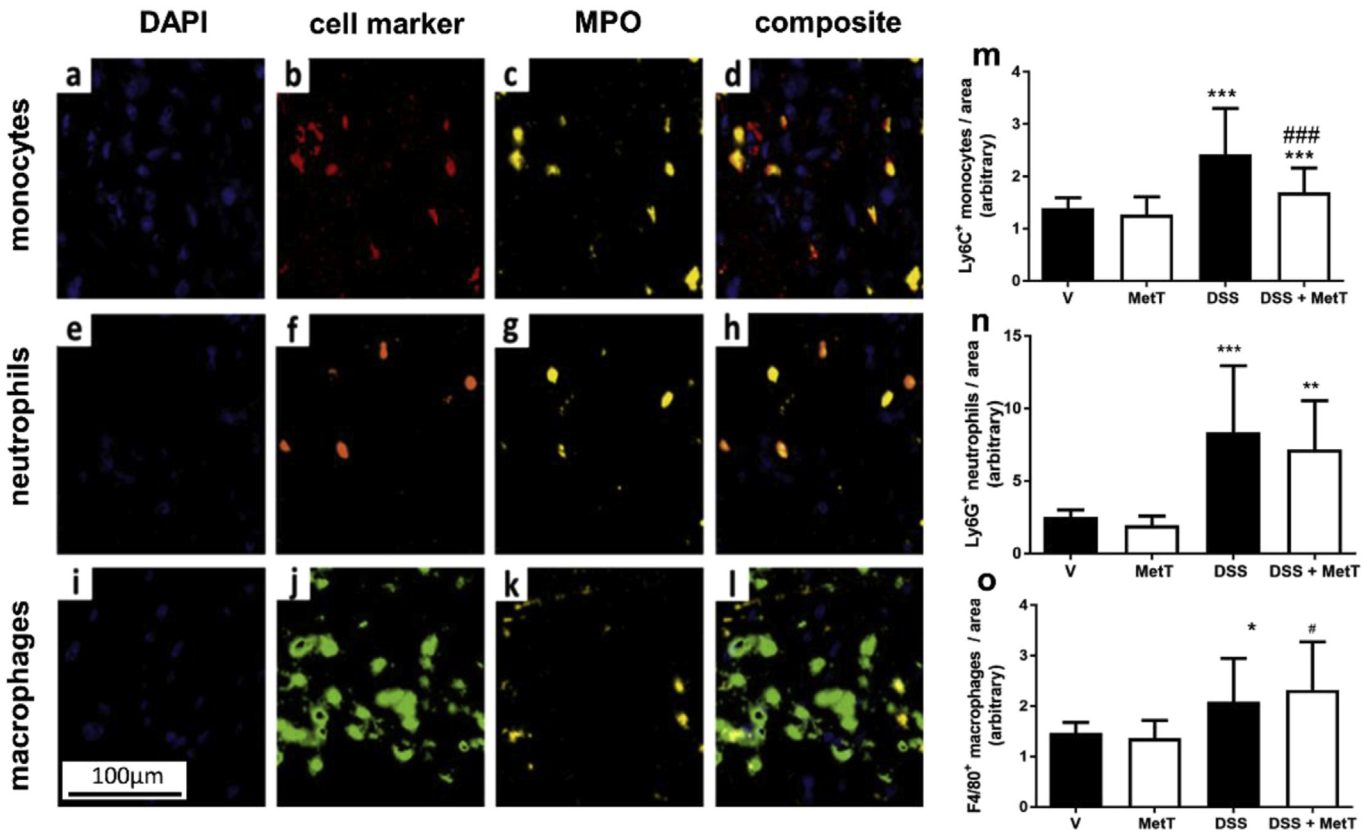

Fig. 5. Representative images of co-labelled MPO with monocytes, neutrophils and macrophages of the inflamed colon following day 9 of DSS challenge. Images were captured at 20x magnification in the inflamed submucosa region and pseudo-coloured in Adobe Photoshop CS6, where nuclei = blue, monocytes = red, neutrophils = orange, macrophages = green and MPO = yellow. Panels depict co-registration of nuclei, cell type and MPO, and also combined images for panels (a–d) monocytes (Ly6C$^+$ immunoreactivity), (e–h) neutrophils (Ly6G + immunoreactivity) and (i–l) macrophages (F4/80$^+$ immunoreactivity). Software-based enumeration shown in panels (m) monocytes, (n) neutrophils and (o) macrophages represent an assessment of cellular count in the colon performed using InForm (V2.1.1) with all data normalised to length of colon per field of view. Data represents approximately n = 50–70 fields of view, per mouse with data averaged and plotted as mean ± SD; n = 6 mice per group. Different to corresponding controls; $^*p < 0.05$; $^{**}p < 0.01$ and $^{***}p < 0.001$. Different to the DSS group in the absence of MetT; $^{\#\#\#}p < 0.001$. Images were digitally magnified from original 20x magnification. Scale bar = 100 µm. (For interpretation of the references to colour in this figure legend, the reader is referred to the Web version of this article.)

immunomodulatory effects [36]. To investigate whether MetT altered the immunological profile of the colon during DSS-induced colitis, the levels of the potent anti-inflammatory cytokine, IL-10, and the pro-inflammatory cytokine IL-6 were assessed. Overall, IL-10 was significantly downregulated (Fig. 8a), while IL-6 showed a significant increase (Fig. 8b) in the colons of both DSS-treated groups (when compared to normal drinking water controls), consistent with other reports of cytokine profiles during acute DSS-induced colitis in the literature [1]. No significant difference in colonic IL-10 or IL-6 was detected between DSS and DSS + MetT treated mice, suggesting that MetT exhibited no immunomodulatory effects during DSS-induced colitis; although, there was a weak trend to decreased IL-6 in DSS + MetT, compared to DSS treated mice (Fig. 8b). The anti-inflammation effects of MetT on DSS-induced colitis observed herein did not appear to be linked to cytokine-induced immunomodulatory effects and therefore the observed protective effects of MetT are likely attributed to its antioxidant activity.

2.9. MetT abrogates DSS-mediated cell death in the inflamed colon

Cell death is characteristic during acute colitis and can be attributed to the oxidative environment [38,54], exacerbating histoarchitectural damage to the colon. We examined cell death by probing fragmented DNA using a TUNEL assay in histologically prepared colon samples. TUNEL$^+$-dead cells were confirmed by bright green fluorescent labelling that was pyknotic in appearance. As expected, there was little colonic TUNEL$^+$-labelling in tissue from the vehicle control group while there was marked increase TUNEL$^+$-labelling in the colons of DSS-treated mice (Fig. 9a). Interestingly, mice co-treated with DSS and MetT showed significantly abrogated levels of TUNEL$^+$ labelling, when compared to mice treated with DSS alone (Fig. 9a and b). Under these conditions, levels of colonic TUNEL$^+$ pixels (as measured via software image analysis using the optical density) in mice co-treated with DSS and MetT were comparable to that of the vehicle group.

3. Discussion

Despite a lack of data to specify a direct cause in IBD, it is clear that mucosal injury and epithelial damage precedes the inflammatory insult that affects the gut microbiota, leading to a characteristic neutrophil infiltration to the submucosa and subsequent ROS production via activated MPO [15]. Available evidence points to markedly increased MPO levels in patients with IBD, and MPO is correlated to disease severity [37,51,58]. For example, neutrophils are congregated within active ulcers in UC and coincide with chemotactic factors (IL-8) that signal neutrophil degranulation leading to MPO release and subsequent HOCl production [4,43]. Unlike other ROS, HOCl is a powerful 2-electron oxidant capable of irreversible oxidation of thiols, lipids and DNA, eventuating in cell death. We have postulated that inhibition of MPO will attenuate the course of acute colitis via combined antioxidant and anti-inflammatory potential [15]. Outcomes from this study show that 4-Methoxy-TEMPO accumulated in the colon (as judged by MALDI-

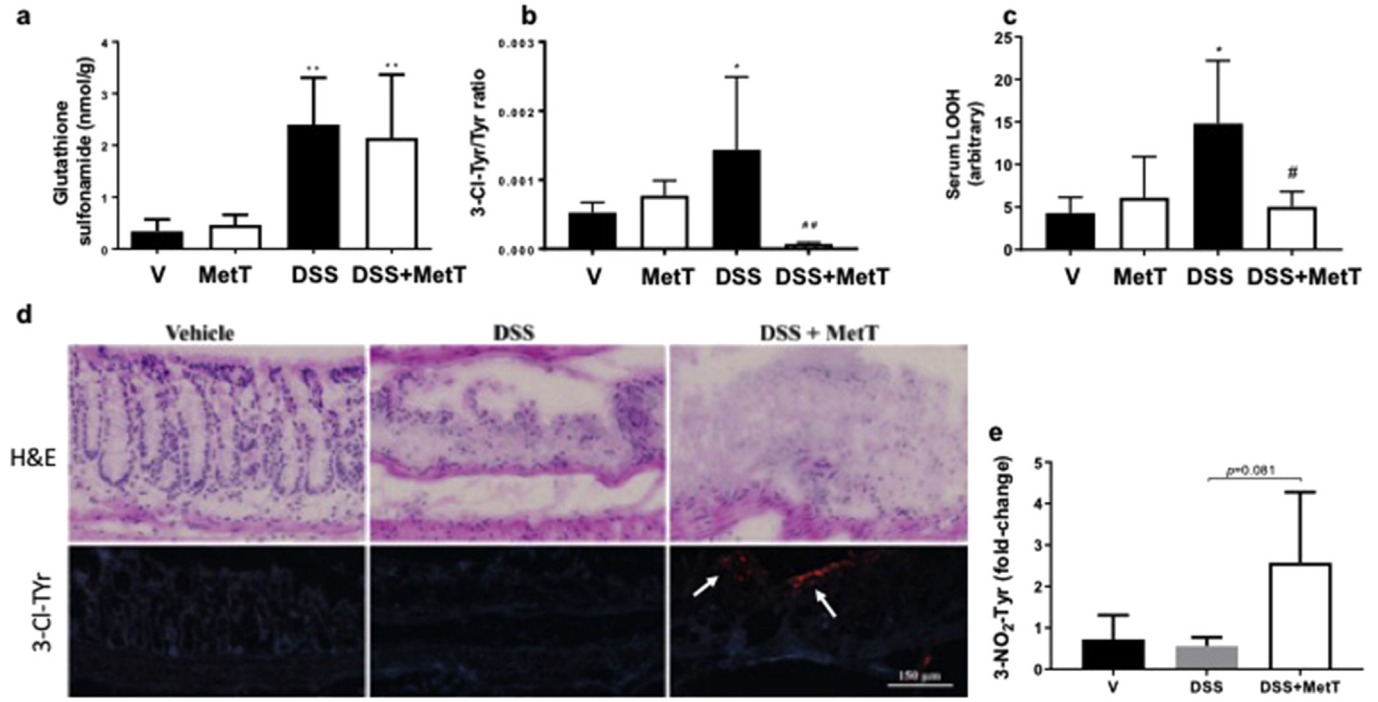

Fig. 6. Biomarkers of MPO-mediated oxidative damage after 9 days of DSS insult. Panels represent (a) glutathione sulfonamide and (b) 3-chloro-tyrosine (3-Cl-Tyr); biomarkers were determined in colon homogenates with LC mass spectrometry analysis, while the lipid (per)oxidation biomarker (c) lipid hydroperoxide (LOOH) was assessed using a modified FOX-1 assay from fresh plasma isolated on day 9 of DSS. Panel (d) shows 3-NO_2-Tyr labelling determined with frozen colon tissue sections immunohistochemically labelled using TSA amplification and juxtaposed to H&E stained serial sections. Arrow indicates 3-NO_2-Tyr^+ labelling (red-fluorescent staining). Panel (e) shows the quantification of 3-NO_2-Tyr^+ labelling performed using the software, MetaMorph® V7.8, with 3-NO_2-Tyr^+ labelling normalised to the length of colon in each field of view and presented as a fold-change relative to the vehicle group. Data represents approximately n = 30 fields of view per mouse with data averaged and plotted as mean ± SD; n = 6 mice per group. Data for glutathione sulfonamide and 3-Cl-Tyr data represent mean ± SD; n = 6 mice per group. Different to corresponding controls; $^{*}p < 0.05$ and $^{**}p < 0.01$. Different to the DSS group in the absence of MetT; $^{\#}p < 0.05$ and $^{\#\#}p < 0.01$. Images were digitally magnified from original 20x magnification. Scale bar = 150 μm. (For interpretation of the references to colour in this figure legend, the reader is referred to the Web version of this article.)

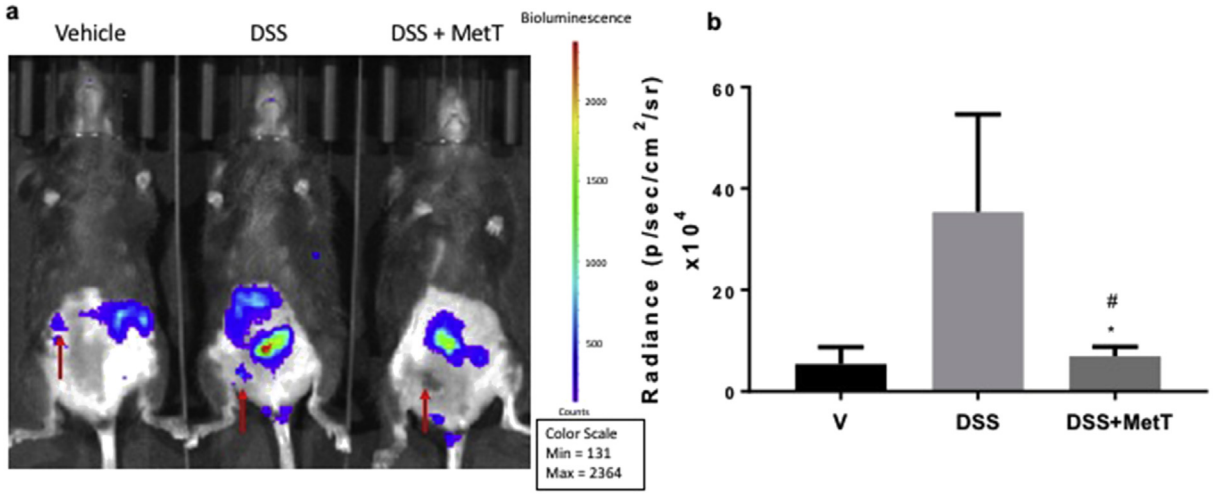

Fig. 7. *In vivo* bioluminescent imaging of oxidised luminol in 8-week-old C57BL/6 wild type female mice receiving either no treatment, dextran sodium sulfate (DSS) alone, or co-administration of DSS and 4-Methoxy-TEMPO (MetT). Mice were anaesthetised with 3% v/v isoflurane and injected (*i.p.*) with either 17 mM MetT or vehicle. Following 5 min and immediately preceding imaging, 100 μL of 374 mM luminol solution was injected subcutaneously in the scruff of mice. Panels show (a) Representative *in vivo* bioluminescent imaging of vehicle (left), DSS (middle) and DSS + MetT (right) mice (red arrows denote site of *i. p.* injection), (b) Quantification of *in vivo* bioluminescent regions of interest (ROIs); note vertical scale to the right of images refers to the relative luminescence radiance presented as a heat map. Data were quantified on peak total bioluminescent signal using Caliper Life Sciences (V4) and represented as radiance in photon/sec/cm^2/sr. Mice were imaged on day 7 of DSS-induced colitis. Images were captured using the IVIS® SpectrumCT In Vivo Imaging System (PerkinElmer). Data represents one technical repeat with vehicle n = 3, DSS n = 3 & DSS + MetT n = 4. Different to corresponding controls; $^{\#}p < 0.05$. Different to the DSS group in the absence of MetT; $^{*}p < 0.05$. (For interpretation of the references to colour in this figure legend, the reader is referred to the Web version of this article.)

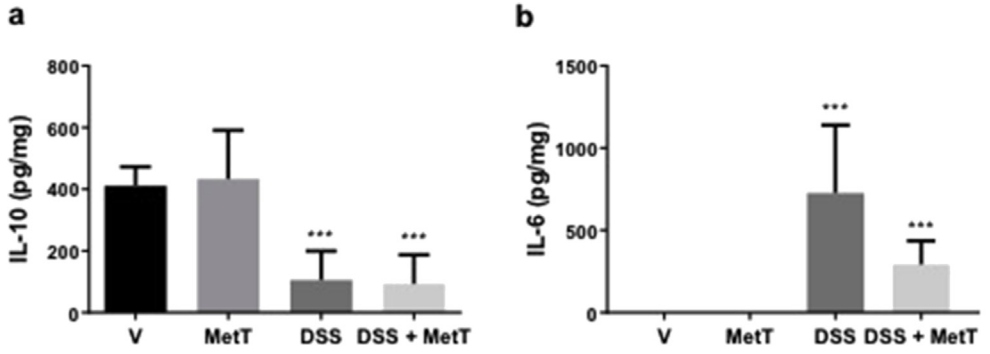

Fig. 8. ELISA-based quantification of cytokines IL-10 and IL-6 in colon tissues following DSS insult. Panel (a) IL-10 & (b) IL-6 in the colon following 9 days of DSS-induced colitis with and without MetT treatment. Data represents mean ± SD; n = 6 mice per group. Different to corresponding controls; $^{***}p < 0.001$.

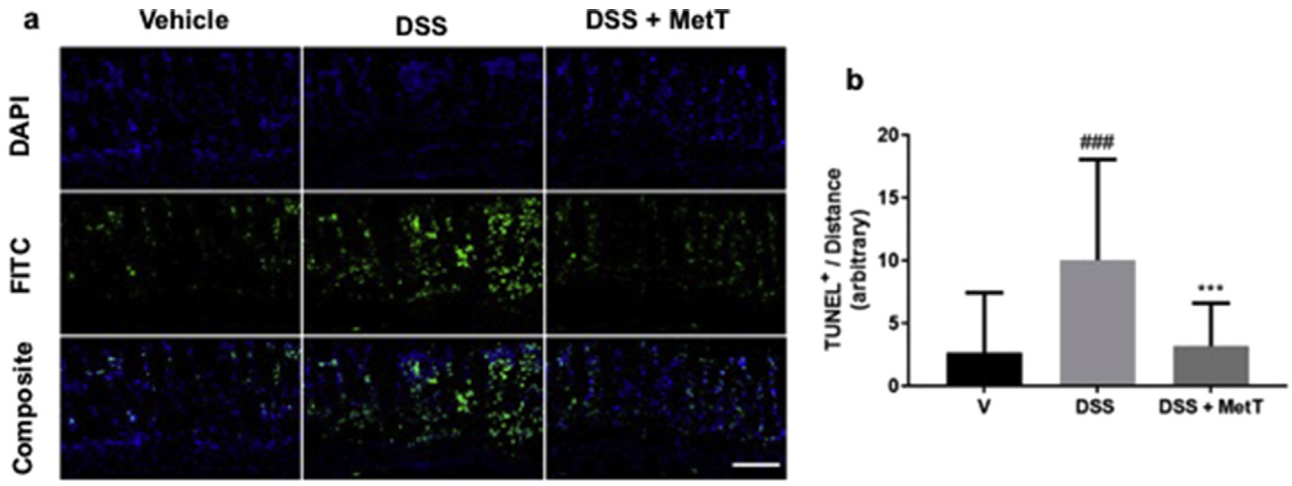

Fig. 9. Representative images and quantification of TUNEL positivity in the colon mucosa following 9 days of DSS challenge. Panels show (a) Representative TUNEL$^+$ labelling of double stranded DNA in the colon mucosa, (b) quantification of TUNEL$^+$ labelling as performed using the software, MetaMorph® V7.8, with total counts normalised to the total length of the same colon expressed in millimetres. Data is averaged and plotted as mean ± SD; n = 6 mice per group. n = 28 field of view (FOV) averaged from 6 mice (H_2O + V), n = 15 FOV averaged from 3 mice (DSS + V) and n = 30 FOV averaged from 6 mice (DSS + MetT). Different to DSS group; $^{***}p < 0.001$. Different to vehicle group (in the absence of MetT); $^{###}p < 0.001$. Images were digitally magnified from original 20x magnification. Scale bar = 200 μm.

mass imaging in colon section) and significantly ameliorates the course of experimental colitis through a combined process of inhibiting MPO-halogenating activity and biomarkers of oxidation that together impact on colonic inflammation. Indices including body weight, clinical score, mucin levels and crypt health were notably improved in mice treated with MetT when compared to counterparts receiving DSS alone. Furthermore, MetT also restored colonic histoarchitecture by promoting cell survival, inhibiting the degree to which immune cells infiltrated into layers of the gut and markedly abrogating levels of 3-Cl-Tyr, a specific HOCl oxidation biomarker, suggesting MetT inhibited MPO/HOCl activity in the colon. Luminol-based live animal imaging of mice also revealed significant attenuation of bioluminescence in the abdomen in mice pre-treated with MetT consistent with MPO-inhibition yielding an attenuation of oxidative damage to the colon. Overall, the nitroxide was well-tolerated in mice and effectively inhibited DSS-stimulated acute colitis.

Inflammation-induced oxidative stress is associated with the induction of apoptotic mechanisms of host cells [19]. Data in this study demonstrates that MetT also abrogates oxidative stress-mediated cell death in our model of acute colitis, likely via its antioxidant effect *in vivo*. The antioxidant effect of cyclic nitroxides have been well documented [3,6,34]. For example, the nitroxide derivative TEMPOL was shown to attenuate indomethacin-induced acute colitis in rats when the nitroxide was delivered intraperitoneally [18]. More recently, orally administered nanoparticles containing a cyclic nitroxide inhibited colitis progression in mice challenged with DSS. Thus, Vong and colleagues demonstrated parallel improvements in histologically scored colitis, decreased pro-inflammatory mediators and inhibited ROS-mediated damage [56]. Despite these beneficial outcomes, a role for MPO activity was not specifically explored by Vong and co-workers and herein we addressed this important question of whether cyclic nitroxides inhibited the MPO halogenation cycle *in vivo*.

Data accumulated herein strongly indicates that the cyclic nitroxide ameliorates MPO-mediated oxidation perhaps through inhibition of its halogenation activity although we have not excluded that MetT can directly scavenge HOCl through successive one-electron oxidation reactions with this hypohalous acid, thereby decreasing HOCl levels generated in the colon and providing protection to the gut in the presence of DSS stimulus. The potential for one-electron oxidation of cyclic nitroxides likely precludes oxidation by HOCl – a 2-electron oxidant [42], thus MetT is unlikely to act by scavenging HOCl. While, pre-treatment with MetT failed to inhibit GSA formation [28], the 3-Cl-Tyr biomarker showed a significant inhibition of damage in the presence of nitroxide. This lack of protection afforded to low-molecular weight thiols relative to protein suggests that MPO-HOCl may selectively target protein oxidation relative to HOCl scavenging by GSH in the inflamed colon. This preference may be explained in the relative compartmentalisation of MPO responsible for HOCl production; that is, MPO-HOCl resides in an extracellular environment where the proportion of protein is high relative to GSH that is present within cells at high millimolar

concentrations.

One paradoxical outcome obtained here is that MetT administration increased levels of 3-NO_2-Tyr in DSS treated mice, while there was no significant increase in 3-NO_2-Tyr levels in mice challenged with DSS alone. Peroxynitrite ($ONOO^-$) is formed by the reaction of NO and $O_2^{-\bullet}$. MPO catalytically consumes NO (in the presence of H_2O_2), thereby removing it from the system [7]. Furthermore, it has been previously reported MPO compounds I, II and III consume $O_2^{-\bullet}$ [35]. Therefore, MPO may be acting as a regulator to $ONOO^-$ levels, since $O_2^{-\bullet}$ is a rate limiting radical in the formation of $ONOO^-$ (and subsequent formation of 3-NO_2-Tyr). In addition, others have shown that compound I directly consumes $ONOO^-$, forming compound II [22]. Our results thus corroborate the findings that MPO regulates the formation of 3-NO_2-Tyr, likely by regulating the bioavailability of NO, $O_2^{-\bullet}$ and $ONOO^-$ and therefore paradoxically, inhibiting the MPO-mediated increases in the levels of 3-NO_2-Tyr.

Here we demonstrated that MetT administration modulates the recruitment of immune cells into various histological regions in the inflamed colon. Using advanced image analysis software (InForm), macrophage distribution was mostly localised to the lamina propria, replacing crypt structures in DSS-treated mice (Supplementary Fig. S2 I). It is unclear whether MetT directly inhibits macrophage chemotaxis to the lamina propria during colitis, or whether MetT preserves crypt integrity thus limiting macrophage infiltration. While a previous *in vitro* report demonstrated reduced neutrophil recruitment during nitroxide treatment, we did not observe modulation of neutrophil recruitment *in vivo* in the inflamed colitis model during treatment with MetT [48]. Instead, we report a significant decrease in monocyte recruitment to the inflamed colon during MetT treatment. Similar to previous investigations [48], we also showed significant attenuation of MPO-chlorinating activity with MetT administration during acute colitis. While Queiroz and colleagues attributed reduced MPO-chlorinating activity to attenuation of neutrophil recruitment in their rat model of carrageenan-induced paw inflammation, our data suggest that monocytes and macrophages are also significant sources of MPO in this experimental model of colitis. Hence, a decrease in local MPO-chlorinating activity can also be attributed to reduced recruitment of other leukocytes containing MPO, such as monocytes. This is consistent with our observation of an overall reduction in MPO-containing cells within the inflamed colon during MetT treatment. Overall, it is likely that MetT directly inhibits MPO-chlorinating activity as we observed significant attenuation of MPO-mediated oxidation of luminol in DSS/MetT-treated mice in live animals and complete abrogation of colonic 3-Cl-Tyr levels, a specific marker for MPO-produced HOCl. While several studies have reported antioxidants to attenuate IL-6 levels during inflammation [25,46], the potential effect of a relatively small and nonsignificant decrease in IL-6 is unlikely to be mediating protective effects during DSS insult.

4. Conclusion

The potential multi-faceted impact of MPO-chlorinating activity during IBD is thought to enhance host-tissue injury and exacerbate inflammation. Cyclic nitroxides are powerful antioxidants with anti-inflammatory activities; nitroxides are also well-tolerated *in vivo* and have been previously shown to attenuate MPO activity. We now demonstrate that administration of the cyclic nitroxide MetT during acute DSS-induced colitis significantly attenuates clinical and biochemical parameters that are typically raised during experimental colitis, likely via inhibiting oxidative damage, as well as diminishing monocyte recruitment to the inflamed mucosa and attenuating MPO-chlorinating activity. Thus, we highlight the therapeutic potential for cyclic nitroxides as an adjunctive therapy potentially allowing for decreased dosages of current immunological drugs used in treating patients with IBD that may provide benefit by decreasing deleterious side-effects of these current treatments.

5. Methods

5.1. Materials

All materials and reagents were sourced from Sigma Aldrich, Australia (unless otherwise stated) and were of the highest quality available. All reactions and incubations were performed at 22 °C, unless otherwise specified.

5.2. Ethics

All experiments were approved and carried out according to the University of Sydney Animal Ethics Committee (AEC#651) guidelines. Mice were housed in environmentally enriched AEC-approved cages in The Charles Perkins Centre Animal Facility. Body weight measurements were performed daily to evaluate the course of experimental colitis. A 10–15% body weight loss signalled the study endpoint. Euthanasia was performed via deep anaesthesia with isoflurane inhalation and subsequent cardiac puncture.

5.3. Mice

Wild type C57BL/6 female mice were obtained from Laboratory Animal Services and were housed in The Charles Perkins Centre Animal Facility where food and water were provided *ad libitum*. Experiments were performed when mice were 8–9 weeks of age with n = 6 mice designated to each respective treatment group.

5.4. Dextran sodium sulfate (DSS) model of colitis

Colitis was induced with 3% DSS (w/v) (ICN Biomedicals, Australasia), delivered in drinking water *ad libitum* for 9 days, as previously described [14]. DSS induces epithelial toxicity in the murine colon, causing 'epithelial denudation' and barrier breakdown to commensal flora [40]. Leukocytes infiltrating the *lamina propria* then encounter a spectrum of commensal bacteria and aggressively initiate pro-inflammatory cell recruitment, resulting in the well-characterised model of DSS-induced acute colitis [24]. Mice designated to the control group were housed under identical conditions and received untreated tap water. The selected dose of 4-Methoxy-TEMPO (15 mg/kg) (MetT) was based on a previous investigation using the closely related compound, TEMPOL [5]. Commercially sourced MetT was reconstituted in 10% dimethyl sulfoxide (w/v) immediately prior to use and was diluted to 17 mM stock solution used to administer to the mice in the designated drug-treatment group. Individual mice were administered 100 μL of the MetT stock solution or vehicle (10% v/v DMSO + 90% v/v phosphate buffered saline) via intraperitoneal injections delivered routinely in the morning (at 8 a.m.) and afternoon (5 p.m.) for each day of DSS challenge. In some experiments DSS challenge was decreased markedly at Day 4 to simulate a recovery model, with mice receiving 0.003% w/v DSS in the drinking water up to day 9.

5.5. Biochemical luminol-based myeloperoxidase assay

A master mix containing either 0.2 μg/mL MPO, HRP or Mb and 0.8 mM (w/v) luminol (either supplemented with 750 mM (w/v) NaCl or dH_2O) was incubated with either 1.35 μM, 6.75 μM or 13.5 μM (v/v) MetT and agitated on an orbital shaker at 150 r.p.m. (15 min at 22 °C). Following this, 0.45 mM (v/v) H_2O_2 was simultaneously added to each well and the bioluminescence signal was measured using the IVIS® SpectrumCT In Vivo Imaging System (PerkinElmer, Australia) every 30 s for 10 min. The luminescence was normalised to total photo flux per well.

5.6. Clinical assessment of colitis

Body weight was measured once daily (8 a.m.), where the body weight loss was measured against the original respective body weight at day 0. Mice were clinically scored at day 9 using a value between 0 and 3 for faecal consistency and rectal bleeding (hematochezia), where 0 = normal, 1 = mild, 2 = moderate and 3 = severe as we described previously [14]. The colon was excised, and length measured from the anus to the caecum following sacrifice at day 9 post-DSS treatment to determine the severity of colitis [61].

5.7. Tissue staining with Alcian blue 8GX + Safranin O

Mucin and cell nuclei were stained with 0.1% Alcian blue 8GX (w/v, E. Gurr Ltd., London, UK) in 3% v/v acetic acid (pH 2.5) and 0.1% v/v Safranin O (w/v, E. Gurr Ltd., London, UK) in 0.1% v/v glacial acetic acid, respectively. Briefly, slides were dewaxed, rehydrated and stained with Alcian blue for 30 min prior to washing in water for 5 min. Slides were counterstained in Safranin O for 10 min, washed in tap water, dehydrated and mounted in DPX medium. Alcian blue 8GX histological staining of mucin was evaluated using the MetaMorph® Microscopy Automation & Image Analysis Software (*V7.8*). The sum of pixel intensity threshold was normalised to colon length comprising both the transverse and descending colon.

5.8. Matrix-assisted laser desorption/ionisation mass spectrometry (MALDI-MS)

The lumen of an intact colon was exposed by cutting longitudinally from the anus to the caecum, whereby it was orientated in a 'swiss roll' and embedded in 100 mg/mL porcine gelatin (w/v in dH_2O) before snap freezing in liquid nitrogen. Twelve μm sections of colon were carefully placed on an Indium-Tin Oxide (ITO) conductive slide and placed in a desiccator for 45 min. The ITO slide was then coated with α-Cyano-4-hydroxycinnamic acid (CHCA) matrix solution (7 mg/mL) in 50:50:0.1 CAN/H_2O/TFA using the automatic spraying device, Image Prep (Bruker Daltonics). The thickness of the matrix layer was monitored by the output from the optical sensor, where the readout of the total matrix layer thickness was approximately 4 V total indicating a relatively even distribution of the matrix onto the tissue surface. The coated tissue sections were dried in the desiccator for 20 min before MALDI-MS analysis [45]. MALDI-MS was performed in the 100–2000 amu range while under 8% laser power, 1000 Hz and a raster width of 50 μm. Following MALDI-MS, the ITO slide was retrieved, washed in 100% ethanol and rehydrated before staining with haematoxylin (Harris) & eosin and coverslipping. Slides were imaged on the ZEISS AxioScan.Z1 using the ZEN Blue™ software (*V2.3*).

5.9. 5-plex Opal™ multicolor immunohistochemistry

The innovative OPAL™ kit developed by PerkinElmer enables immunohistochemical labelling of up to 7 markers using the Tyramide Signal Amplification (TSA) working principle. Fluorescently labelled TSA molecules covalently bind to antibody-peroxidase complexes to form a scaffold complex around surrounding antibodies and parts of the antigen. Antibodies, which bind epitopes via Van Der Waals forces, are cleaved in a subsequent microwaving step, leaving behind a TSA scaffold. A new antibody is then incubated, and the cycle is repeated until the desired number of antigens have been labelled. Following sacrifice, colons were removed, flushed with cold PBS, cut longitudinally and orientated into a Swiss Roll prior to overnight fixation in 70% ethanol at 4 °C. The tissue was then processed, embedded in paraffin and sectioned at 5 μm before de-paraffinization and rehydration through a series of graded alcohols. Slides were then placed in a plastic Coplin jar with PBS and microwaved for 15 min at 1000 W to quench endogenous peroxidases. Endogenous Fc receptors were blocked for 30 min using Fc Receptor Blocker (Innovex, CA, USA). Primary antibodies, including anti-F4/80 (BM8, final dilution 1:700 v/v), anti-Ly6C (HK1.4, BioLegend, CA, USA, 1:500 v/v), anti-Ly6G (1A8, BioLegend, CA, USA, 1:500 v/v) and anti-MPO (Abcam, UK, 1:500 v/v) were incubated in separate microwave cycles for 1 h. Peroxidase conjugated anti-rabbit IgG (1:200 v/v) was incubated for 30 min following primary antibody incubation and TBS-T wash steps. Fluorescently conjugated TSA molecules (1:50 v/v) were then incubated for 10 min in the following combinations with primary antibodies: F4/80, TSA-Fluorescein; Ly6G, TSA-Cyanine 3; Ly6C, Cyanine 3.5; MPO, Cyanine 5. After the final microwave cycle, slides were counterstained with DAPI and mounted with ProLong Diamond Antifade Mountant (ThermoFisher, Australia).

5.10. Software-based analysis

OPAL™-labelled colons were imaged on the PerkinElmer Mantra™ microscope with a nuance camera at 20*x* magnification and spectrally unmixed in the InForm (*V2.1.1*) software to obtain a composite image. Composite images were selected at random to train the recognition of crypts, cellular infiltrates and muscularis propria in the automated tissue segmentation feature to 90% confidence, and to assign TSA fluorophores to their respective antibodies for automated cell phenotyping. Histoarchitectural features identified in tissue segmentation analyses were expressed as a percentage against the total volume of tissue detected per field. Enumeration of cell phenotyping was obtained by expressing a particular cell type as the actual counts against total area of colon detected per field.

5.11. Colon biochemistry

Excised colons were flushed with cold PBS and snap frozen in liquid nitrogen before pulverisation by pestle and mortar. Complete lysis buffer (40 mM PBS containing: 1*x* tablet Protease cocktail inhibitor in 50 mL, 10 μM butylated hydroxytoluene w/v, and 1 mM ethylenediaminetetraacetic acid) was added to each pulverised sample, and the slurry transferred to a Teflon-lined test tube and homogenised with a matching piston for 4 min at 500 r.p.m. After processing, colon homogenates were centrifuged at 1600 *g* for 15 min at 4 °C to obtain a clarified supernatant fraction (free of large insoluble tissue debris) that was then stored in aliquots at -80 °C and designated for biochemical analyses.

Where required, total protein content of clarified lysates obtained from colon tissue homogenates were determined using a bicinchoninic acid (BCA) assay, as per manufacturer's instructions. Bovine serum albumin (BSA) was used to generate a standard curve to determine lysate protein concentrations and these values were subsequently used to normalise all biochemical parameters.

5.12. Assessment of glutathione sulfonamide with stable isotope dilution tandem mass spectrometry

Production of glutathione sulfonamide (GSA) from GSH is a specific marker for HOCl presence [27]. Isotopically labelled internal glutathione sulfonamide standard was added to clarified colon lysates containing 300 μg protein. Ice-cold ethanol was added to a final concentration of 80% v/v and incubated for 20 min at -20 °C to precipitate protein. The samples were centrifuged at 16000 *g* for 5 min and glutathione sulfonamide in the supernatant was analysed by LC-MS/MS with single reaction monitoring (SRM) as described previously [28]. LC-MS/MS analyses were performed using a Hypercarb column (150 × 2.1 mm, 3 μm, Thermo Scientific, Waltham, MA) operated at 60° by an Ultimate 3000 RS HPLC system (Thermo Fisher Scientific, Waltham, MA) coupled to a 4000 QTrap mass spectrometer (Sciex, Framingham, MA, USA).

5.13. Assessment of colonic 3-chlorotyrosine with quantitative mass spectrometry

Where required, the HOCl specific protein oxidation marker, *3-chlorotyrosine (*3-Cl-Tyr), was determined as previously described [52]. Briefly, colonic homogenates were homogenised as described earlier and were delipidated with 3% w/v sodium deoxycholate and precipitated with 50% w/v trichloroacetic acid prior to centrifugation at 6000*g* for 5 min. The subsequent pellets underwent an acetone wash with centrifugation (6000 *g* for 5 min), where acetone was removed, and pellets dried under a stream of $N_{2(g)}$. Pellets were then resuspended with 6 M methanesulfonic acid containing 0.2% tryptamine. Internal standards of 3-chloro-[13C9,15 N] tyrosine and [15 N]-tyrosine (final concentration 1.5 nmol) were added to each sample before hydrolysis under vacuum at 110 °C for 12 h.

Quantitative mass spectrometry was employed to quantify 3-chlorotyrosine, as previously described [53]. Hydrolysates were subjected to solid-phase extraction purification using 100% methanol-activated columns (Supelco, Sydney, Australia), before preconditioning with 0.1% v/v TFA/H_2O. Each column was loaded with sample and washed with 2 mL of 0.1% v/v TFA/H_2O and eluted with 80% v/v methanol/H_2O. Columns were dried under vacuum at 60 °C, and re-dissolved in 100 μL of 0.1% v/v formic acid. Tyrosine and 3-Cl-Tyr were quantified using authentic Tyr and 3-Cl-Tyr (0–500 pmol), expressed as a ratio to their corresponding isotopically labelled forms present at 1.5 nmol detected by an Agilent LC-MS system. Levels of Cl-Tyr and Tyr as determined by their corresponding internal standard, which was used to graph the 3-Cl-Tyr/Tyr ratio (Supplementary Fig. S4).

5.14. Modified FOX-1 assay

Serum lipid hydroperoxide (LOOH) was measured using a modified FOX-1 assay, as described previously [8]. Briefly, fresh blood was obtained via cardiac puncture into tubes containing heparin and immediately centrifuged at 3000 *g* for 10 min to isolate plasma. An aliquot of plasma (25 μL) was removed and incubated with 1 μL 4 μM butylated hydroxytoluene (w/v) for 15 min at 22 °C. FOX-1 solution [44] (275 μL) was then added and allowed to incubate for 10 min, before absorbance changes were monitored at 560 nm.

5.15. Immunohistochemical staining of 3-nitrotyrosine

Frozen colon sections were sectioned at 7 μm thickness, stored overnight in -80 °C and thawed (22 °C, 30 min). The slides were then immersed in -30 °C acetone (100%) and incubated for 10 min, followed by two quick washes with dH_2O. The sections were then heat antigen retrieved in 10 mM sodium citrate (pH 6) solution using a microwave for 30 min. Following this, slides were allowed to warm to 22 °C before application of an endogenous FcR blocker (Innovex Biosciences, CA, USA; NB309) for 45 min, followed by a TBS-T wash (3*x* 2 min). Anti-3-NO_2-Tyr antibody was incubated over sections for 60 min at 22 °C (1:200 v/v; Sigma Aldrich, Australia; N0409), followed by a TBS-T wash (3*x* 2 min). Peroxidase conjugated anti-rabbit IgG (1:200 v/v) was then added to sections and incubated for an additional 30 min before slides were washed in TBS-T (4*x* 2 min). Following this, sections were incubated for 10 min in a dark humidity chamber with a 1:50 v/v solution of TSA fluorophore (PerkinElmer, Australia; FP1488) before washing with TBS-T (4*x* 2 min). Finally, a solution of DAPI (1:1000 v/v; PerkinElmer, Australia; FP1490) was applied to slides for 5 min in a dark humidity chamber prior to washing with TBS-T (4*x* 2 min) and cover-slipping with mounting medium (Dako, Australia; S3023). Images were acquired using a wide-field epi-fluorescent microscope (ZEN) and Anti-3-NO_2-Tyr labelling was evaluated using the MetaMorph® Microscopy Automation & Image Analysis Software (*V7.8*). The sum of pixel intensity threshold was normalised to colon length comprising both the transverse and descending colon.

5.16. In vivo imaging of oxidised luminol

At day 7 of DSS-induced colitis, mice were sedated with 3% (v/v) isoflurane and anaesthesia was maintained with 1.5% (v/v) isoflurane within the IVIS® SpectrumCT In Vivo Imaging System chamber housed in the University of Sydney, Sydney Preclinical Imaging Facility. Prior to imaging, Nair™ Tough Hair Removal Cream was applied to the abdomen of mice and incubated for 3 min before removal with a warm wet gauze to expose the bare abdomen. Next, MetT or vehicle was delivered via *i. p.* injection following 15 min before subcutaneous injection of 300 mg/kg (w/v) luminol delivered into the scruff of mice and allowed to be absorbed systemically for 5 min [26]. Following this procedure, the bioluminescent signal from mice abdomens (maximum 5 mice in the visualising chamber) were detected with a 3 min exposure time (F/stop = 1; binning = 16). Finally, 2D planar bioluminescence images were presented as radiance in photon/sec/cm^2/sr and regions of interest (ROIs) were quantified on peak total bioluminescent signal using Caliper Life Sciences (*V4*).

5.17. ELISA assessment of pro-inflammatory mediators

Sandwich ELISA kits were purchased from elisakit.com (elisakit.com, Australia) and were performed according to the manufacturer's instructions. Briefly, 20 μL of clarified colon lysate (or standard) was added to pre-coated and pre-blocked wells in duplicate and incubated overnight at 4 °C. The samples/standards were subsequently removed, and all wells were washed (3*x* 3 min) in washing buffer prior to incubation with 50 μL of anti-IL-10 or IL-6 (1:1000 v/v) for 1 h. The detection antibodies were then discarded and wells washed (3*x* 3 min) prior to incubation with 50 μL of streptavidin/horseradish peroxidase (final dilution 1:5000 v/v) for 45 min. Following washing steps, 50 μL of tetramethylbenzidine was added to each well and colorimetric development continued for 30 min in the dark. The reaction was halted by addition of sulfuric acid (50 μL, 1 M) and absorbance measured at 450 nm. All data was normalised to total protein content and presented in absolute or relative values.

5.18. Immunofluorescent staining of TUNEL$^+$ cells

A commercial DNA fragmentation (TUNEL) assay kit (Abcam, Australia; ab66110) was used to stain for TUNEL$^+$ cells in frozen colon sections. Slides were fixed in 4% (w/v) formaldehyde in PBS and incubated for 15 min, followed by two repeats of washing (5 min each) with PBS. Each tissue section was then covered with 100 μL of 20 μg/mL Proteinase K solution (10 mg/mL Proteinase K, 100 mM Tris-HCl pH 8.0, 50 mM EDTA) and incubated for 5 min. Colon sections were then transferred to 4% (w/v) formaldehyde in PBS and incubated for 5 min and subsequently immersed and incubated in PBS for another 5 min. Slides were then removed from PBS and gently tapped on the benchtop to remove excess liquid.

Colon sections were covered with 100 μL Wash Buffer and incubated for 5 min and this was repeated once more. Slides were covered with 50 μL of DNA Labelling Solution (per test: 10 μL TdT Reaction Buffer, 0.75 μL TdT Enzyme, 8 μL Br-dUTP, 32.25 μL ddH_2O) and placed inside a dark humidity incubator at 37 °C for 1 h. The slides were then taken out and washed twice with PBS (5 min per wash). 100 μL of Antibody Solution (per test: 5 μL Anti-BrdU-Red Antibody, 95 μL Rinse Buffer) was then used to cover each slide and incubated away from light (30 min, 22 °C). Sections were then washed with dH_2O for 5 min, followed by counterstaining with Spectral DAPI (PerkinElmer, USA; FP1490) for 10 min and cover-slipped with fluorescence mounting medium (Dako, Australia; S3023). Slides were viewed using the Zeiss Axio Scope. A1 microscope and images captured at 10x magnification with the ZEN 2 blue edition imaging software. Subsequent quantification of TUNEL$^+$ staining was conducted on MetaMorph® software (*V7.6*).

5.19. Statistical analysis

Statistical analysis was performed using GraphPad Prism (V5), and data were evaluated using one-way ANOVA with Tukey post-hoc test for multiple comparisons (for comparing three or more groups and accounting for type 1 and type 2 statistical error); significance was accepted at the 95% confidence level ($p < 0.05$). Where relevant, data is presented as mean ± SD with the number of repetitions and p values (≤ 0.05, 0.01 or 0.001) indicated in the Figure legends.

Conflicts of interest

None of the authors have any disclosures to industry or other sponsor that represent a conflict of interest.

Acknowledgements

The authors acknowledge funding from the Australian Research Council (DP0878559 and DP160102063 grants and NHMRC Project Grant 1125392 awarded to PKW). Mass spectrometry was performed at the Bosch Mass Spectrometry Facility (quantitative mass spectrometry) or at the Sydney Mass Spectrometry Facility (MALDI-mass mapping). We thank Dr Leo Phillips from the Sydney Mass Spectrometry Facility for assistance and advice with the MALDI-mass imaging analyses that were carried out at this core research facility at the University of Sydney. Non-invasive imaging was conducted at the Charles Perkins Centre Preclinical Imaging Facility.

Appendix A. Supplementary data

Supplementary data to this article can be found online at https://doi.org/10.1016/j.redox.2019.101333.

References

[1] P. Alex, N.C. Zachos, T. Nguyen, L. Gonzales, T.E. Chen, L.S. Conklin, M. Centola, X. Li, Distinct cytokine patterns identified from multiplex profiles of murine dss and tnbs-induced colitis, Inflamm. Bowel Dis. 15 (2009) 341–352.
[2] H.A. Almenier, H.H. Al Menshawy, M.M. Maher, S. Al Gamal, Oxidative stress and inflammatory bowel disease, Front. Biosci. 4 (2012) 1335–1344.
[3] N. Alrabadi, B. Chami, B.H. Kim, A. Min Maw, M.A. Dennis, K.P. Witting, Hypochlorous acid generated in the heart following acute ischaemic injury promotes myocardial damage: a new target for therapeutic development, Trends Cell Mol. Biol. (2014) In Press.
[4] K. Anezaki, H. Asakura, T. Honma, K. Ishizuka, K. Funakoshi, Y. Tsukada, R. Narisawa, Correlations between interleukin-8, and myeloperoxidase or luminol-dependent chemiluminescence in inflamed mucosa of ulcerative colitis, Intern. Med. 37 (1998) 253–258.
[5] Y. Araki, H. Sugihara, T. Hattori, The free radical scavengers edaravone and tempol suppress experimental dextran sulfate sodium-induced colitis in mice, Int. J. Mol. Med. 17 (2006) 331–334.
[6] O. Augusto, D.F. Trindade, E. Linares, S.M. Vaz, Cyclic nitroxides inhibit the toxicity of nitric oxide-derived oxidants: mechanisms and implications, An. Acad. Bras. Cienc. 80 (2008) 179–189.
[7] S. Baldus, T. Heitzer, J.P. Eiserich, D. Lau, H. Mollnau, M. Ortak, S. Petri, B. Goldmann, H.J. Duchstein, J. Berger, U. Helmchen, B.A. Freeman, T. Meinertz, T. Munzel, Myeloperoxidase enhances nitric oxide catabolism during myocardial ischemia and reperfusion, Free Radic. Biol. Med. 37 (2004) 902–911.
[8] D. Banerjee, U.K. Madhusoodanan, M. Sharanabasappa, S. Ghosh, J. Jacob, Measurement of plasma hydroperoxide concentration by FOX-1 assay in conjunction with triphenylphosphine, Clin. Chim. Acta 337 (2003) 147–152.
[9] J.S. Beckman, T.W. Beckman, J. Chen, P.A. Marshall, B.A. Freeman, Apparent hydroxyl radical production by peroxynitrite: implications for endothelial injury from nitric oxide and superoxide, Proc. Natl. Acad. Sci. U. S. A. 87 (1990) 1620–1624.
[10] J.S. Beckman, Oxidative damage and tyrosine nitration from peroxynitrite, Chem. Res. Toxicol. 9 (1996) 836–844.
[11] D.F. Berg, A.M. Bahadursingh, D.L. Kaminski, W.E. Longo, Acute surgical emergencies in inflammatory bowel disease, Am. J. Surg. 184 (2002) 45–51.
[12] R.M. Brand, M.W. Epperly, J.M. Stottlemyer, E.M. Skoda, X. Gao, S. Li, S. Huq, P. Wipf, V.E. Kagan, J.S. Greenberger, L.D. Falo JR., A topical mitochondria-targeted redox-cycling nitroxide mitigates oxidative stress-induced skin damage, J. Investig. Dermatol. 137 (2017) 576–586.
[13] E.P. Brestel, Co-oxidation of luminol by hypochlorite and hydrogen peroxide implications for neutrophil chemiluminescence, Biochem. Biophys. Res. Commun. 126 (1985) 482–488.
[14] B. Chami, A.W. Yeung, C. Van Vreden, N.J. King, S. Bao, The role of CXCR3 in DSS-induced colitis, PLoS One 9 (2014) e101622.
[15] B. Chami, N.J.J. Martin, J.M. Dennis, P.K. Witting, Myeloperoxidase in the inflamed colon: a novel target for treating inflammatory bowel disease, Arch. Biochem. Biophys. 645 (2018) 61–71.
[16] D. Cuscela, D. Coffin, G.P. Lupton, J.A. Cook, M.C. Krishna, R.F. Bonner, J.B. Mitchell, Protection from radiation-induced alopecia with topical application of nitroxides: fractionated studies, Cancer J. Sci. Am. 2 (1996) 273–278.
[17] M.J. Davies, C.L. Hawkins, D.I. Pattison, M.D. Rees, Mammalian heme peroxidases: from molecular mechanisms to health implications, Antioxidants Redox Signal. 10 (2008) 1199–1234.
[18] H. Deguchi, K. Yasukawa, T. Yamasaki, F. Mito, Y. Kinoshita, T. Naganuma, S. Sato, M. Yamato, K. Ichikawa, K. Sakai, H. Utsumi, K. Yamada, Nitroxides prevent exacerbation of indomethacin-induced gastric damage in adjuvant arthritis rats, Free Radic. Biol. Med. 51 (2011) 1799–1805.
[19] T.L. Denning, H. Takaishi, S.E. Crowe, I. Boldogh, A. Jevnikar, P.B. Ernst, Oxidative stress induces the expression of Fas and Fas ligand and apoptosis in murine intestinal epithelial cells, Free Radic. Biol. Med. 33 (2002) 1641–1650.
[20] A. Dhanasekaran, S. Kotamraju, C. Karunakaran, S.V. Kalivendi, S. Thomas, J. Joseph, B. Kalyanaraman, Mitochondria superoxide dismutase mimetic inhibits peroxide-induced oxidative damage and apoptosis: role of mitochondrial superoxide, Free Radic. Biol. Med. 39 (2005) 567–583.
[21] A.M. El-Tawil, A population-based case-control study of potential risk factors for IBD, Am. J. Gastroenterol. 104 (2009) 1064.
[22] S. Galijasevic, D. Maitra, T. Lu, I. Sliskovic, I. Abdulhamid, H.M. Abu-Soud, Myeloperoxidase interaction with peroxynitrite: chloride deficiency and heme depletion, Free Radic. Biol. Med. 47 (2009) 431–439.
[23] E. Gaudio, G. Taddei, A. Vetuschi, R. Sferra, G. Frieri, G. Ricciardi, R. Caprilli, Dextran sulfate sodium (DSS) colitis in rats: clinical, structural, and ultrastructural aspects, Dig. Dis. Sci. 44 (1999) 1458–1475.
[24] D.R. Getts, R.L. Terry, M.T. Getts, C. Deffrasnes, M. Muller, C. Van Vreden, T.M. Ashhurst, B. Chami, D. Mccarthy, H. Wu, J. Ma, A. Martin, L.D. Shae, P. Witting, G.S. Kansas, J. Kuhn, W. Hafezi, I.L. Campbell, D. Reilly, J. Say, L. Brown, M.Y. White, S.J. Cordwell, S.J. Chadban, E.B. Thorp, s. Bao, S.D. Miller, N.J. King, Therapeutic inflammatory monocyte modulation using immune-modifying microparticles, Sci. Transl. Med. 6 (2014) 219ra7.
[25] J.P. Godbout, B.M. Berg, K.W. Kelley, R.W. Johnson, alpha-Tocopherol reduces lipopolysaccharide-induced peroxide radical formation and interleukin-6 secretion in primary murine microglia and in brain, J. Neuroimmunol. 149 (2004) 101–109.
[26] S. Gross, S.T. Gammon, B.L. Moss, D. Rauch, J. Harding, J.W. Heinecke, L. Ratner, D. Piwnica-Worms, Bioluminescence imaging of myeloperoxidase activity in vivo, Nat. Med. 15 (2009) 455–461.
[27] D.T. Harwood, A.J. Kettle, C.C. Winterbourn, Production of glutathione sulfonamide and dehydroglutathione from GSH by myeloperoxidase-derived oxidants and detection using a novel LC-MS/MS method, Biochem. J. 399 (2006) 161–168.
[28] D.T. Harwood, A.J. Kettle, S. Brennan, C.C. Winterbourn, Simultaneous determination of reduced glutathione, glutathione disulphide and glutathione sulphonamide in cells and physiological fluids by isotope dilution liquid chromatography-tandem mass spectrometry, J Chromatogr B Analyt Technol Biomed Life Sci 877 (2009) 3393–3399.
[29] J. Hcanin-endres, B. Salky, F. Gattorno, M. Edye, Laparoscopically assisted intestinal resection in 88 patients with Crohn's disease, Surg. Endosc. 13 (1999) 595–599.
[30] J.W. Heinecke, W. LI, H.L. Daehnke 3rd, J.A. Goldstein, Dityrosine, a specific marker of oxidation, is synthesized by the myeloperoxidase-hydrogen peroxide system of human neutrophils and macrophages, J. Biol. Chem. 268 (1993) 4069–4077.
[31] L. Huang, G. Wojciechowski, P.R. Ortiz De Montellano, Prosthetic heme modification during halide ion oxidation. Demonstration of chloride oxidation by horseradish peroxidase, J. Am. Chem. Soc. 127 (2005) 5345–5353.
[32] J.M. Hwang, M.G. Varma, Surgery for inflammatory bowel disease, World J. Gastroenterol. 14 (2008) 2678–2690.
[33] V.E. Kagan, j. Jiang, h. Bayir, D.A. Stoyanovsky, Targeting nitroxides to mitochondria: location, location, location, and ...concentration: highlight commentary on "Mitochondria superoxide dismutase mimetic inhibits peroxide-induced oxidative damage and apoptosis: role of mitochondrial superoxide", Free Radic. Biol. Med. 43 (2007) 348–350.
[34] T.B. Kajer, K.E. Fairfull-Smith, T. Yamasaki, K. Yamada, S. Fu, S.E. Bottle, C.L. Hawkins, M.J. Davies, Inhibition of myeloperoxidase- and neutrophil-mediated oxidant production by tetraethyl and tetramethyl nitroxides, Free Radic. Biol. Med. 70 (2014) 96–105.
[35] A.J. Kettle, R.F. Anderson, M.B. Hampton, C.C. Winterbourn, Reactions of superoxide with myeloperoxidase, Biochemistry 46 (2007) 4888–4897.
[36] C.H. Kim, J.B. Mitchell, C.A. Bursill, A.L. Sowers, A. Thetford, J.A. Cook, D.M. Van Reyk, M.J. Davies, The nitroxide radical TEMPOL prevents obesity, hyperlipidaemia, elevation of inflammatory cytokines, and modulates atherosclerotic plaque composition in apoE-/- mice, Atherosclerosis 240 (2015) 234–241.
[37] C.G. Knutson, A. Mangerich, Y. Zeng, A.R. Raczynski, R.G. Liberman, P. Kang, W. YE, E.G. Prestwich, K. Lu, J.S. Wishnok, J.R. Korzenik, G.N. Wogan, J.G. Fox, P.C. Dedon, S.R. Tannenbaum, Chemical and cytokine features of innate immunity characterize serum and tissue profiles in inflammatory bowel disease, Proc. Natl. Acad. Sci. U. S. A. 110 (2013) E2332–E2341.
[38] L. Kruidenier, I. Kuiper, C.B. Lamers, H.W. Verspaget, Intestinal oxidative damage in inflammatory bowel disease: semi-quantification, localization, and association with mucosal antioxidants, J. Pathol. 201 (2003) 28–36.
[39] J.S. Levine, R. Burakoff, Extraintestinal manifestations of inflammatory bowel

disease, Gastroenterol. Hepatol. 7 (2011) 235–241.
[40] J. Luther, S.Y. Owyang, T. Takeuchi, T.S. Cole, M. Zhang, M. Liu, J. Erb-Downward, J.H. Rubenstein, C.C. Chen, A.V. Pierzchala, J.A. Paul, J.Y. Kao, Helicobacter pylori DNA decreases pro-inflammatory cytokine production by dendritic cells and attenuates dextran sodium sulphate-induced colitis, Gut 60 (2011) 1479–1486.
[41] J.M. Metz, D. Smith, R. Mick, R. Lustig, J. Mitchell, M. Cherakuri, E. Glatstein, S.M. Hahn, A phase I study of topical Tempol for the prevention of alopecia induced by whole brain radiotherapy, Clin. Cancer Res. 10 (2004) 6411–6417.
[42] S. Morris, G. Sosnovsky, B. Hui, C.O. Huber, N.U. Rao, H.M. Swartz, Chemical and electrochemical reduction rates of cyclic nitroxides (nitroxyls), J. Pharm. Sci. 80 (1991) 149–152.
[43] D. Muthas, A. Reznichenko, C.A. Balendran, G. Bottcher, I.G. Clausen, C. Karrman Mardh, T. Ottosson, M. Uddin, T.T. Macdonald, S. Danese, M. Berner Hansen, Neutrophils in ulcerative colitis: a review of selected biomarkers and their potential therapeutic implications, Scand. J. Gastroenterol. 52 (2017) 125–135.
[44] K.J. Nelson, D. Parsonage, Measurement of peroxiredoxin activity, Curr Protoc Toxicol (2011), https://doi.org/10.1002/0471140856.tx0710s49 (Chapter 7), Unit 7.10.
[45] A. Nilsson, T.E. Fehniger, L. Gustavsson, M. Andersson, K. Kenne, G. Marko-Varga, P.E. Andren, Fine mapping the spatial distribution and concentration of unlabeled drugs within tissue micro-compartments using imaging mass spectrometry, PLoS One 5 (2010) e11411.
[46] M. Penkowa, J. Hidalgo, Metallothionein treatment reduces proinflammatory cytokines IL-6 and TNF-alpha and apoptotic cell death during experimental autoimmune encephalomyelitis (EAE), Exp. Neurol. 170 (2001) 1–14.
[47] W.A. Prutz, Hypochlorous acid interactions with thiols, nucleotides, DNA, and other biological substrates, Arch. Biochem. Biophys. 332 (1996) 110–120.
[48] R.F. Queiroz, A.K. Jordao, A.C. Cunha, V.F. Ferreira, M.R. Brigagao, A. Malvezzi, A.T. Amaral, O. Augusto, Nitroxides attenuate carrageenan-induced inflammation in rat paws by reducing neutrophil infiltration and the resulting myeloperoxidase-mediated damage, Free Radic. Biol. Med. 53 (2012) 1942–1953.
[49] M.D. Rees, S.E. Bottle, K.E. Fairfull-Smith, E. Malle, J.M. Whitelock, M.J. Davies, Inhibition of myeloperoxidase-mediated hypochlorous acid production by nitroxides, Biochem. J. 421 (2009) 79–86.
[50] J.A. Roberts, L. Durnin, K.A. Sharkey, V.N. Mutafova-Yambolieva, G.M. Mawe, Oxidative stress disrupts purinergic neuromuscular transmission in the inflamed colon, J. Physiol. 591 (2013) 3725–3737.
[51] T. Saiki, Myeloperoxidase concentrations in the stool as a new parameter of inflammatory bowel disease, Kurume Med. J. 45 (1998) 69–73.
[52] A. Shanu, L. Groebler, H.B. Kim, S. Wood, C.M. Weekley, J.B. Aitken, H.H. Harris, P.K. Witting, Selenium inhibits renal oxidation and inflammation but not acute kidney injury in an animal model of rhabdomyolysis, Antioxidants Redox Signal. 18 (2013) 756–769.
[53] J. Talib, D.I. Pattison, J.A. Harmer, D.S. Celermajer, M.J. Davies, High plasma thiocyanate levels modulate protein damage induced by myeloperoxidase and perturb measurement of 3-chlorotyrosine, Free Radic. Biol. Med. 53 (2012) 20–29.
[54] T. Tian, Z. Wang, J. Zhang, Pathomechanisms of oxidative stress in inflammatory bowel disease and potential antioxidant therapies, Oxid Med Cell Longev 2017 (2017) 4535194.
[55] S.M. Vaz, F.M. Prado, P. Di Mascio, O. Augusto, Oxidation and nitration of ribonuclease and lysozyme by peroxynitrite and myeloperoxidase, Arch. Biochem. Biophys. 484 (2009) 127–133.
[56] L.B. Vong, T. Tomita, T. Yoshitomi, H. Matsui, Y. Nagasaki, An orally administered redox nanoparticle that accumulates in the colonic mucosa and reduces colitis in mice, Gastroenterology 143 (2012) 1027–1036 e3.
[57] T. Vowinkel, T.J. Kalogeris, M. Mori, C.F. Krieglstein, D.N. Granger, Impact of dextran sulfate sodium load on the severity of inflammation in experimental colitis, Dig. Dis. Sci. 49 (2004) 556–564.
[58] M. Wagner, C.G. Peterson, P. Ridefelt, P. Sangfelt, M. Carlson, Fecal markers of inflammation used as surrogate markers for treatment outcome in relapsing inflammatory bowel disease, World J. Gastroenterol. 14 (2008) 5584–5589 discussion 5588.
[59] J. Wilson, C. Hair, R. Knight, A. Catto-Smith, S. Bell, M. Kamm, P. Desmond, J. Mcneil, W. Connell, High incidence of inflammatory bowel disease in Australia: a prospective population-based Australian incidence study, Inflamm. Bowel Dis. 16 (2010) 1550–1556.
[60] R.J. Xavier, D.K. Podolsky, Unravelling the pathogenesis of inflammatory bowel disease, Nature 448 (2007) 427–434.
[61] Y. Xu, N.H. Hunt, S. Bao, The role of granulocyte macrophage-colony-stimulating factor in acute intestinal inflammation, Cell Res. 18 (2008) 1220–1229.
[62] X.R. Xu, C.Q. Liu, B.S. Feng, Z.J. Liu, Dysregulation of mucosal immune response in pathogenesis of inflammatory bowel disease, World J. Gastroenterol. 20 (2014) 3255–3264.
[63] T. Yonetani, H. Schleyer, Studies on cytochrome c peroxidase. IX. The reaction of ferrimyoglobin with hydroperoxides and a comparison of peroxide-induced compounds of ferrimyoglobin and cytochrome c peroxidase, J. Biol. Chem. 242 (1967) 1974–1979.
[64] B. Zofia, Kate Summers, Stephen Bevan, Working Well: Promoting Job and Career Opportunities for Those with IBD. Lancaster University, The Work Foundation, 2015.